Rail. Eng. Science (2021) 29(2):199–210
https://doi.org/10.1007/s40534-021-00236-z

Simplified analytical solution for stress concentration ratio of piled embankments incorporating pile–soil interaction

Qiang Luo[1,2] · Ming Wei[1] · Qingyuan Lu[1] · Tengfei Wang[1,2]

Received: 20 January 2021 / Revised: 3 March 2021 / Accepted: 5 March 2021 / Published online: 11 May 2021

Abstract Piled embankments have been extensively used for high-speed rail over soft soils because of their effectiveness in minimizing differential settlement and shortening the construction period. Stress concentration ratio, defined as the ratio of vertical stress carried by pile heads (or pile caps if applicable) to that by adjacent soils, is a fundamental parameter in the design of piled embankments. In view of the complicated load transfer mechanism in the framework of embankment system, this paper presents a simplified analytical solution for the stress concentration ratio of rigid pile-supported embankments. In the derivation, the effects of cushion stiffness, pile–soil interaction, and pile penetration behavior are considered and examined. A modified linearly elastic-perfectly plastic model was used to analyze the mechanical response of a rigid pile–soil system. The analytical model was verified against field data and the results of numerical simulations from the literature. According to the proposed method, the skin friction distribution, pile–soil relative displacement, location of neural point, and differential settlement between the pile head (or cap) and adjacent soils can be determined. This work serves as a fast algorithm for initial and reasonable approximation of stress concentration ratio on the design aspects of piled embankments.

Keywords Piled embankments · Pile–soil interaction · Pile penetration · Cushion · Rigid pile · High-speed railway

✉ Tengfei Wang
w@swjtu.edu.cn

[1] School of Civil Engineering, Southwest Jiaotong University, Chengdu 610031, China

[2] MOE Key Laboratory of High-Speed Railway Engineering, Southwest Jiaotong University, Chengdu 610031, China

1 Introduction

High-speed railway network in China is the world's longest and most extensively used—with a total length of 37,900 km by the end of 2020. Owing to the continuing development of high-speed rail projects in China and other countries, track substructures require careful attention to ensure the safe delivery of passengers [1]. In the case of a high-speed rail embankment, two major challenges may arise when weak foundation soil occurs: low strength and high compressibility of weak soils that poses geotechnical problems to infrastructures and control of post-construction settlement [2, 3]. Embankment reinforced with rigid piles has been universally recognized as an effective solution to minimize the settlement of weak subsoil, which contributes greatly to deformation [4–7].

Typical piled embankment primarily comprises piles, pile caps, an angular platform consisting of gravels and geosynthetics (if applicable), and an overlying embankment fill, as shown in Fig. 1. The law of stress redistribution among all these components can be complex owing to the interactions within the earthwork system [8]. Extensive investigations have been performed to elucidate the load transfer mechanism of piled embankments (e.g., [9–11]) for design purposes. Some analytical and numerical models [12–20] have been developed based on diversified assumptions to account for the soil arching effect at the base of embankments, classified into categories such as limit equilibrium, frictional, and rigid models. However, some fundamental factors may be overlooked in these models (e.g., cushion layer, geosynthetic reinforcement, and load transfer efficiency of pile–soil system) when evaluating the mechanical behavior of piled embankments. Hence, some theoretical methods [8, 21–23] have been developed to analyze the pile–soil interaction below the

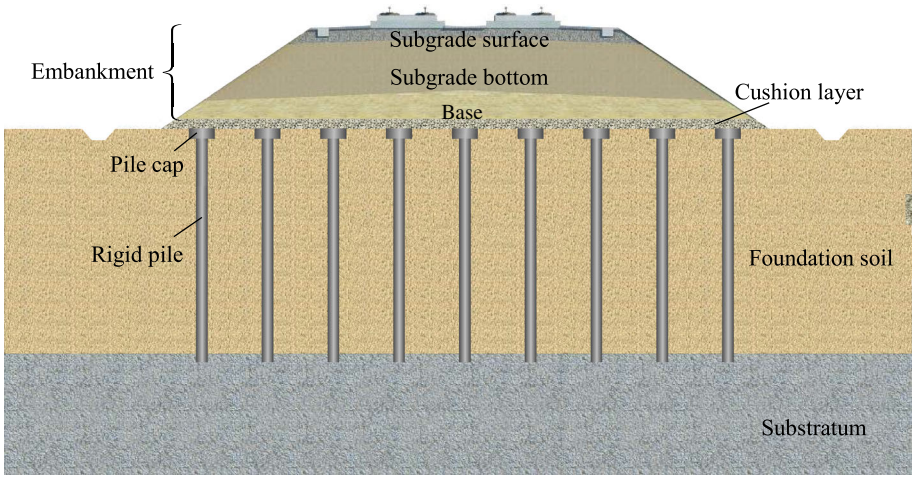

Fig. 1 Profile of a rigid pile-supported embankment system for high-speed rail

base of embankments, which can be divided into two main categories: semi-analytical method and closed-form solution. Although these approaches can be used to reveal the deformation characteristics of piles and the surrounding soil, they are not applicable when considerable loads are anticipated under high fill [24]. In addition, the role of the cushion layer, which is critical in interpreting the mechanical behavior of foundation reinforced by rigid piles, is ignored in some of the mentioned methods.

Stress concentration ratio is taken as a fundamental parameter in design of piled embankments and is a key indicator of the deformation and bearing capacity of underlying reinforced foundation; however, few methods are available for reasonably estimating its value. Combined with recent advances in elucidating the load transfer mechanism of piled embankments [25, 26], this paper presents a novel analytical solution for predicting the stress concentration ratio. The main advantages of the proposed method over conventional methodologies include proper consideration of cushion stiffness and pile penetration behavior. Besides, a modified linearly elastic-perfectly plastic model was employed to determine the shear resistance and deformation at the pile–soil interface. Based on the improved interface model, negative skin friction along pile shafts can be captured, and more rational skin friction distribution is obtained considering the variation of soil stress level. The proposed method was verified against the results of numerical analysis and field measurements from two case histories.

2 Skin friction distribution

2.1 Pile–soil interface model

The mobilization of skin friction along the pile shaft primarily depends on the shear characteristics of the pile–soil interface. Numerous investigations have been conducted to obtain the stress–strain relationship for the soil–structure interface, providing theoretical descriptions such as exponential, linearly elastic-perfectly plastic, hyperboloid, and bilinear models. In this study, the linearly elastic-perfectly plastic model was selected as the pile–soil interface model owing to its computational simplicity and reasonable accuracy [8, 21, 22, 27, 28].

Within the theoretical framework of the linearly elastic-perfectly plastic model, two parameters, i.e., shear stiffness (K_s) and ultimate shear strength of the soil–pile interface (τ_u), must be determined. Chen et al. [8] illustrated that both parameters would increase with depth and lateral earth pressure; however, an empirical formula [29] (see Eq. (1)) has been more widely used in many studies (e.g., [21, 22, 30]) to calculate K_s with the shear modulus of surrounding soil (G_s) being a constant.

$$K_s = \frac{\tau_u}{U_{z,c}} = \frac{2G_s l}{r_p^2 \ln(r_m/r_p)}, \tag{1}$$

where $U_{z,c}$ is the critical shear displacement; l and r_p are the values of pile length and radius, respectively; r_m is the influential radius of the pile in terms of soil domain. As specified in Fig. 2a, K_s is independent of depth.

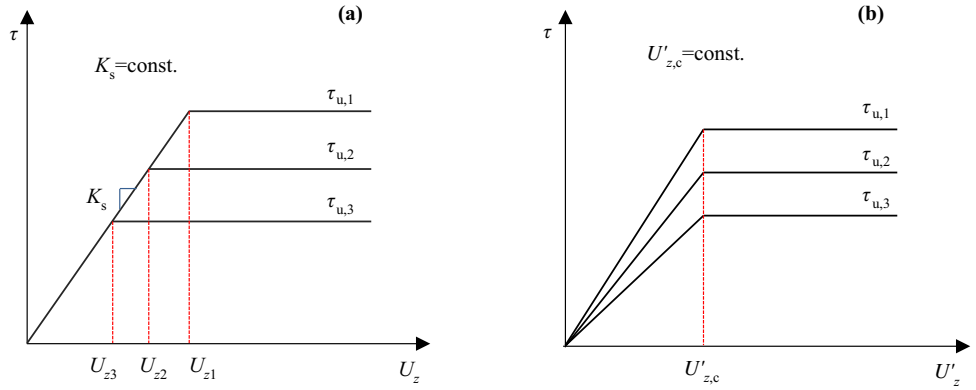

Fig. 2 Linearly elastic-perfectly plastic model for pile–soil interaction in two forms: **a** constant shear stiffness; **b** normalized critical shear displacement as a constant

The results of shear tests on the sand–steel interface, performed by Evgin and Fakharian [31], indicate that the normal stress level is slightly related to $U_{z,c}$ but is significantly related to the K_s. It appears more appropriate to adopt a constant critical shear displacement in the formulation of the elastic-perfectly plastic model [32–34]. In addition, the sample size was reported to significantly affect the critical shear displacement of a shear stress–displacement curve obtained from direct shear tests [35]. Consequently, the concept of normalized shear displacement, U_z/L (L represents the box dimension in the shear direction), was introduced to eliminate the effect of sample size in the determination of a representative critical shear displacement, as shown in Fig. 2b. In general, the skin friction between construction material and soil is governed by material type, soil properties, and the roughness [36]. The parameters for describing the shear behavior at the soil–structure interface are available in literature.

Considering the discussions above, a load transfer model was established based on normalized shear displacement. Hence, the modified shear stiffness (K_s') at the pile–soil interface can be calculated by

$$K_s'(z) = \frac{\tau_u(z)}{U'_{z,c}}, \tag{2}$$

where $U'_{z,c}$ denotes the critical relative displacement at the pile–soil interface per unit length; $\tau_u(z)$ is the ultimate skin friction as a function of depth (i.e., z), expressed by

$$\tau_u(z) = c_a + K_0(\gamma z + p_s)\tan\varphi_a, \tag{3}$$

where K_0 is the lateral earth pressure coefficient; γ is the unit weight of adjacent soil; p_s represents the vertical stress applied to the soil mass; c_a and φ_a correspond to the adhesion and friction angle of the soil–pile interface, respectively, which can be estimated using the strength reduction method as follows (in case experimental data are not accessible):

$$c_a = R_{in}c_s, \tag{4a}$$

$$\tan\varphi_a = R_{in}\tan\varphi_s \le \tan\varphi_s, \tag{4b}$$

where R_{in} is the strength reduction factor; c_s and φ_s are the effective cohesion component and effective friction angle of the adjacent soil, respectively. In general, the value of R_{in} is 2/3 for sand–steel interface and 1/2 for the clay–steel interface, and a rough interface results in a larger R_{in}.

2.2 Mobilization of skin friction

For a rigid pile-supported embankment, stress concentration occurs at the pile cap (or pile head) under an embankment load. The pile cap would penetrate upward into the cushion layer in extreme conditions, and a negative skin friction can be anticipated along the upper portion of the pile shaft. Below the neural plane, positive skin friction is mobilized to resist the downward movement of the rigid pile. Assuming that the pile–soil interaction follows the linearly elastic-perfectly plastic model, pile tip penetration occurs once the lower pile–soil interface reaches a critical state. The pile basal resistance is then mobilized to counteract the loads from the upper structure and the positive skin friction. In general, the skin friction along the pile shaft can be divided into three segments, corresponding to I, II, and III in Fig. 3a. Within Segments I and III, the shear behavior of the pile–soil interface has reached the plastic stage, while the pile–soil interface undergoes an elastic deformation in Segment II. It was assumed that U_z' varied linearly with depth in Segment II, which was consistent with the findings of Chen et al. [8]. Therefore, the mathematical expression for U_z' can be obtained as

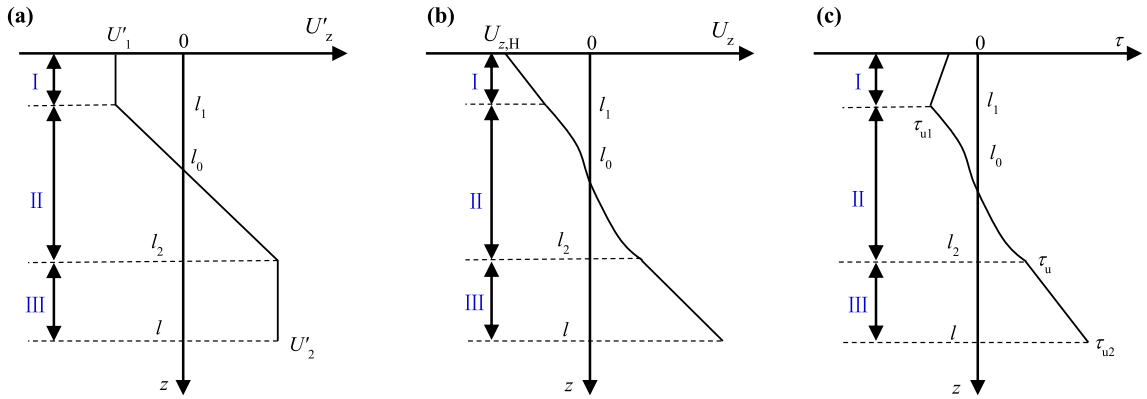

Fig. 3 Profiles of relative displacement per unit length (**a**), relative displacement (**b**), and skin friction (**c**) on the pile shaft

$$U_z' = \begin{cases} -U_1' & (0 \le z \le l_1) \\ \dfrac{z - l_0}{l_0 - l_1} U_1' & (l_1 \le z \le l_0) \\ \dfrac{z - l_0}{l_2 - l_0} U_2' & (l_0 \le z \le l_2) \\ U_2' & (l_2 \le z \le l) \end{cases}, \tag{5}$$

where z is the depth (the elevation of the pile head as the reference level); U_1' and U_2' are the critical relative displacements per unit length related to the soil type and properties of the pile surface, respectively; l is the pile length; l_1 and l_2 are the locations of the demarcation point. It is noteworthy that $U_1' = U_2'$ if the subsoil is homogeneous.

According to the geometrical relationship in Fig. 3a, we have

$$\frac{l_0 - l_1}{l_2 - l_0} = \frac{U_1'}{U_2'}. \tag{6}$$

Integrating for the area under the curve in Fig. 3a results in an expression for the distribution of pile–soil relative displacement (U_z), as graphically represented in Fig. 3b. The pile–soil relative displacement at the pile head ($U_{z,H}$) can be inferred as

$$U_{z,H} = \frac{U_1'}{2}(l_1 + l_0). \tag{7}$$

Combining Eqs. (2), (3), and (5) yields (see Fig. 3c)

$$\tau(z) = \begin{cases} -A - Bz & (0 \le z \le l_1) \\ \dfrac{Bz^2 + (A - Bl_0)z - Al_0}{l_0 - l_1} & (l_1 \le z \le l_0) \\ \dfrac{Bz^2 + (A - Bl_0)z - Al_0}{l_2 - l_0} & (l_0 \le z \le l_2) \\ A + Bz & (l_2 \le z \le l) \end{cases}, \tag{8}$$

where $A = c_a + K_0 p_s \tan \varphi_a$ and $B = K_0 \gamma \tan \varphi_a$.

3 Stress concentration ratio

3.1 Element selection from a piled embankment system

It is typical to use geosynthetic basal reinforcement in piled embankments for high-speed rail. Several studies have suggested that geosynthetic reinforcement has limited effect on both the stress concentration ratio and maximum settlement of an embankment when the tensile stiffness of the geosynthetic material is less than 860 kN/m [9, 37] or when the pile spacing is sufficiently close [38]. However, some researchers [12, 13, 39] argued that geosynthetic reinforcement is crucial for determining the stress concentration ratio. Given the abovementioned controversy and China's TB 10001–2016 design code, this paper focuses on the pile–soil interaction in the following sections; therefore, necessary simplifications will be performed regarding soil arching and the effect of geosynthetic reinforcement.

The pile groups are generally arranged in a regular spacing pattern, and the pile spacing is significantly smaller compared with the span of an embankment. The performances of a pile–soil system under an embankment load can be treated as the same, except for those beneath the slope [40, 41]. Therefore, a cylindrical unit cell was introduced, as shown in Fig. 4. The equivalent diameter $d_e = 2b$ representing the affected region can be calculated by [42]

$$d_e = 2b = c_g S, \tag{9}$$

where b is the equivalent radius of a cylindrical unit cell; S denotes the pile spacing; c_g represents the shape factor of 1.05 and 1.13 for triangular and square arrangements, respectively.

The following assumptions and simplifications were made in the derivation of the analytical solution:

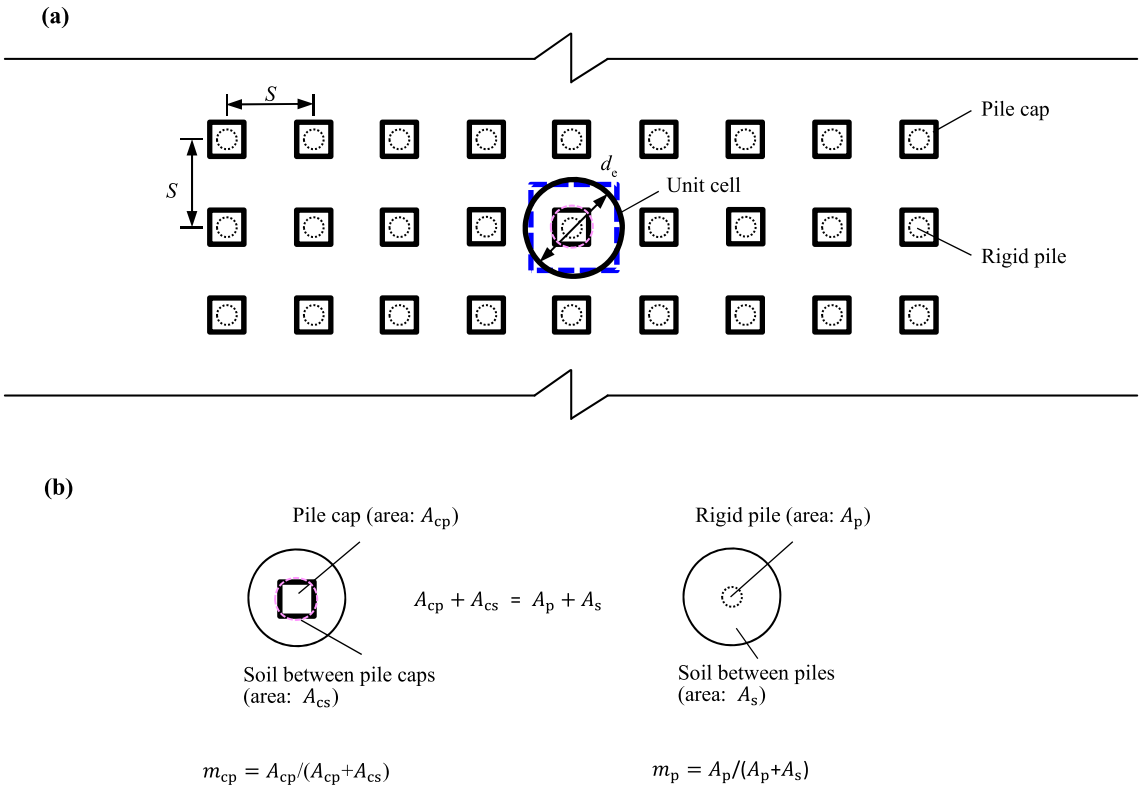

Fig. 4 Selected element for the analysis of pile–soil interaction: **a** top view at the elevation level of pile cap; **b** area calculation in terms of pile cap, pile head, and surrounding soil

(a) A one-dimensional compression problem is considered for the system.
(b) The embankment load is treated as a uniformly distributed vertical load, p.
(c) The pressures acting on the pile cap and soil mass are uniformly distributed (closely spaced plies).
(d) The pile configurations are identical, and a linear elastic and isotropic material is used for the pile.
(e) The penetration resistance at the pile cap and pile tip varies linearly with the penetration level. Nonlinear behavior and punching shear failure of cushion, and retraining effect of geosynthetics reinforcement in high fill conditions are not involved.
(f) The foundation is regarded as a perfectly elastoplastic material, and the self-weight of the rigid pile is ignored.

Based on the assumptions, a relationship can be established among p, p_p, and p_s (see Fig. 4b):

$$p = m_{cp}p_p + (1 - m_{cp})p_s, \tag{10}$$

where p_p and p_s denote the pressure on the pile cap and soil surface beneath the cushion layer, respectively; $m_{cp} = A_{cp}/(A_{cp} + A_{cs})$ defines the area percentage for the pile cap; A_{cp} and A_{cs} are the cross-sectional areas of the pile cap and projected area of soil, respectively.

3.2 Stress and deformation of pile and soil

As demonstrated in Fig. 5, elements of the pile and soil mass having a thickness of dz were considered for mechanical analysis. The force equilibrium equations yields

$$\begin{cases} \dfrac{d\sigma_p(z)}{dz} = -\dfrac{2}{a}\tau(z) \\ \dfrac{d\sigma_s(z)}{dz} = \dfrac{a}{b^2}\tau(z) \end{cases}, \tag{11}$$

where a represents the pile shaft diameter; b denotes the outer diameter of the soil element; σ_p and σ_s are the vertical stresses of the pile and soil, respectively.

Substituting Eq. (8) in Eq. (11) and then integrating Eq. (11) on both sides with respect to the variable z yields

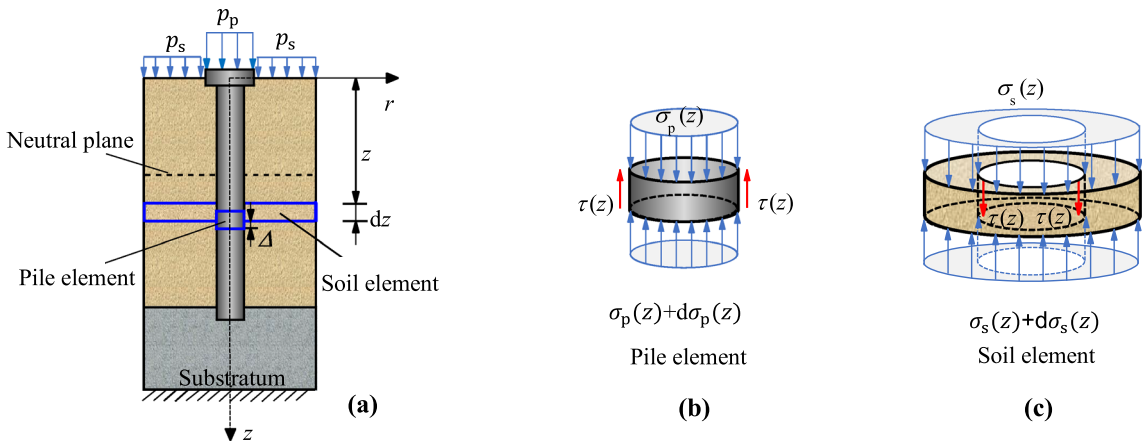

Fig. 5 Schematic of force equilibrium analysis (**a**) for a given pile element (**b**) and soil element (**c**) under one-dimensional compression

$$\sigma_{pi}(z)=\begin{cases}\frac{B}{a}z^2+\frac{2A}{a}z+C_1 & (i=1)\\ -\frac{2}{a(l_0-l_1)}\left(\frac{B}{3}z^3+\frac{A-Bl_0}{2}z^2-Al_0z\right)+C_2 & (i=2)\\ -\frac{2}{a(l_2-l_0)}\left(\frac{B}{3}z^3+\frac{A-Bl_0}{2}z^2-Al_0z\right)+C_3 & (i=3)\\ -\frac{B}{a}z^2-\frac{2A}{a}z+C_4 & (i=4)\end{cases}, \tag{12}$$

$$\sigma_{si}(z)=\begin{cases}-\frac{aB}{2b^2}z^2-\frac{aA}{b^2}z+C_5 & (i=1)\\ \frac{a}{b^2(l_0-l_1)}\left(\frac{B}{3}z^3+\frac{A-Bl_0}{2}z^2-Al_0z\right)+C_6 & (i=2)\\ \frac{a}{b^2(l_2-l_0)}\left(\frac{B}{3}z^3+\frac{A-Bl_0}{2}z^2-Al_0z\right)+C_7 & (i=3)\\ \frac{aB}{2b^2}z^2+\frac{aA}{b^2}z+C_8 & (i=4)\end{cases}, \tag{13}$$

where σ_{pi} and σ_{si} are the vertical stresses of the pile and soil, respectively; C_1-C_8 are integral constants; subscript $i=1,2,3,4$ corresponds to the depth $z\in(0,l_1),(l_1,l_0),(l_0,l_2),(l_2,l)$, respectively.

Integrating Eq. (12) yields

$$\begin{aligned}w_{pu}&=\int_0^{l_1}\frac{\sigma_{p1}(z)}{E_p}dz+\int_{l_1}^{l_0}\frac{\sigma_{p2}(z)}{E_p}dz\\&=\frac{B(l_0^4-l_1^4)+4A(l_0^3-l_1^3)}{6a(l_0-l_1)E_p}+\frac{C_1l_1+C_2(l_0-l_1)}{E_p},\end{aligned} \tag{14a}$$

$$\begin{aligned}w_{pb}&=\int_{l_0}^{l_2}\frac{\sigma_{p3}(z)}{E_p}dz+\int_{l_2}^{l}\frac{\sigma_{p4}(z)}{E_p}dz\\&=-\frac{(3A+Bl)l^2}{3aE_p}+\frac{B(l_2^4-l_0^4)+4A(l_2^3-l_0^3)}{6aE_p(l_2-l_0)}\\&\quad+\frac{C_3(l_2-l_0)+C_4(l-l_2)}{E_p},\end{aligned} \tag{14b}$$

where w_{pu} and w_{pb} represent the compressive deformation of the pile shaft above and below the neutral plane, respectively; E_p is the elastic modulus of the pile material.

Similarly, integrating Eq. (13) yields the expression for the compressive deformation of soil mass above and below the neutral plane, w_{su} and w_{sb}, respectively:

$$\begin{aligned}w_{su}&=\int_0^{l_1}\frac{\sigma_{s1}(z)}{E_s}dz+\int_{l_1}^{l_0}\frac{\sigma_{s2}(z)}{E_s}dz\\&=-\frac{aB(l_0^4-l_1^4)+4aA(l_0^3-l_1^3)}{12b^2(l_0-l_1)E_s}+\frac{C_5l_1+C_6(l_0-l_1)}{E_s},\end{aligned} \tag{15a}$$

$$\begin{aligned}w_{sb}&=\int_{l_0}^{l_2}\frac{\sigma_{s3}(z)}{E_s}dz+\int_{l_2}^{l}\frac{\sigma_{s4}(z)}{E_s}dz\\&=\frac{(3A+Bl)al^2}{6b^2E_s}-\frac{aB(l_2^4-l_0^4)+4aA(l_2^3-l_0^3)}{12b^2E_s(l_2-l_0)}\\&\quad+\frac{C_7(l_2-l_0)+C_8(l-l_2)}{E_s},\end{aligned} \tag{15b}$$

where E_s is the constrained modulus of adjacent soil. For layered soil, E_s can be estimated by [43]

$$E_s=\frac{1}{l}\sum_{i=1}^{n}E_{si}h_i, \tag{16}$$

where E_{si} and h_i are the constrained modulus and thickness of the corresponding soil layer, respectively.

3.3 Boundary and compatibility conditions

Following the previous assumptions, the penetration of the pile head/cap (x_{pu}) and pile tip (x_{pb}) can be obtained as

$$x_{pu}=C_c\left[\sigma_p(z)-\sigma_s(z)\right]|_{z=0}, \tag{17a}$$

$$x_{pb}=C_r\left[\sigma_p(z)-\sigma_s(z)\right]|_{z=l}, \tag{17b}$$

where C_c and C_r are the flexibility factors (m/kPa) for the cushion layer and substratum, respectively. They reflect the effect of the cushion layer on the mechanical performance

of the pile–soil system. According to Eqs. (12) and (13), $\sigma_p(l)$ and $\sigma_s(l)$ can be determined as follows:

$$\begin{cases} \sigma_p(l) = -\dfrac{B}{a}l^2 - \dfrac{2A}{a}l + C_4 \\ \sigma_s(l) = \dfrac{aB}{2b^2}l^2 + \dfrac{aA}{b^2}l + C_8 \end{cases}. \tag{18}$$

The stress boundary conditions for the pile and soil mass at the elevation level of the pile cap ($z = 0$) can be expressed as (referring to Fig. 4)

$$\begin{cases} \sigma_p(0) = \dfrac{p_p A_{cp}}{A_p} = \dfrac{p_p m_{cp}}{m_p} \\ \sigma_s(0) = \dfrac{p_s A_{cs}}{A_s} = \dfrac{p_s(1-m_{cp})}{(1-m_p)} \end{cases}, \tag{19}$$

where $m_p = A_p/(A_p + A_s)$ is defined as the ratio of the pile head area to the total area; A_p and A_s are the cross-sectional areas of the pile shaft and surface area of the adjacent soil, respectively.

The pile penetration at the elevation of the cushion layer ($z = 0$) is equal to the relative displacement between pile and the adjacent soil of $z = 0$. Combining Eqs. (7) and (17) yields

$$\sigma_p(0) - \sigma_s(0) = \frac{U_1'}{2C_c}(l_1 + l_0). \tag{20}$$

The following equations can be obtained as per compatibility conditions for Eqs. (12) and (13):

$$\begin{aligned} &\sigma_{p1}(l_1) = \sigma_{p2}(l_1),\ \sigma_{p2}(l_0) = \sigma_{p3}(l_0),\ \sigma_{p3}(l_2) = \sigma_{p4}(l_2); \\ &\sigma_{s1}(l_1) = \sigma_{s2}(l_1),\ \sigma_{s2}(l_0) = \sigma_{s3}(l_0),\ \sigma_{s3}(l_2) = \sigma_{s4}(l_2). \end{aligned} \tag{21}$$

Given the dimensions and physical properties of the cushion layer, the compressive deformation of the cushion layer is not evaluated in deriving the displacement compatibility equations. However, it is noteworthy that the deformation effect of the cushion layer on the behavior of the pile–soil system can be observed in Eq. (17), in the form of a counter force acting on the pile cap. Based on the displacement compatibility condition (Fig. 6), the following can be inferred:

$$\begin{cases} w_{su} + w_{sb} = s_{s1} - s_{s2} \\ w_{pu} + w_{pb} = s_{p1} - s_{p2} \\ s_{s1} = s_{p1} + x_{pu} \\ s_{p2} = s_{s2} + x_{pb} \end{cases}, \tag{22}$$

where s_{s1} and s_{p1} are the settlements of the soil surface and pile cap, respectively; s_{p2} and s_{s2} denote the settlements of the pile tip and upper surface of the substratum, respectively. Because no differential settlement occurs at the neural plane, the transformation of Eq. (22) yields

$$w_{su} - w_{pu} = x_{pu}, \tag{23a}$$

$$w_{sb} - w_{pb} = x_{pb}. \tag{23b}$$

3.4 Solution for stress concentration ratio

In summary, 13 variables must be determined, i.e., integral constants C_1−C_8 from Eqs. (12) and (13); and l_1, l_0, l_2, p_s, and p_p. They can be solved analytically based on Eqs. (6), (10), (19)–(21), and (23) because the system is consistent. These 13 equations are highly nonlinear, rendering it challenging to solve using an explicit method. Consequently, reducing the number of unknown variables becomes top priority; in fact, C_1−C_8, p_s, and p_p can be expressed by l_1, l_0, and l_2. Subsequently, a numerical technique known as the Newton–Raphson method is used to solve the system of equations. The general procedure is as follows:

i. Combining Eqs. (10), (19), and (20) yields

$$\begin{cases} p_p = \dfrac{m_p p}{m_{cp}} + \dfrac{m_p U_1'(1-m_p)(l_1+l_0)}{2C_c m_{cp}} \\ p_s = \dfrac{(1-m_p)p}{1-m_{cp}} - \dfrac{m_p U_1'(1-m_p)(l_1+l_0)}{2C_c(1-m_{cp})} \end{cases}, \tag{24}$$

ii. Substituting Eqs. (12) and (13) in Eqs. (19) and (21), respectively, and then combining them with Eq. (24) yields the expressions for C_1−C_8 in terms of l_1, l_0, and l_2.

iii. Substituting Eqs. (14a), (15a), and (17a) in Eq. (23a) yields the first equation of system.

iv. Substituting Eqs. (14b), (15b), and (17b) in Eq. (23b) yields the second equation of system.

v. Eq. (6) is the third equation of system; the combination of the three equations is then solved using the commercial software MATHEMATICA.

Stress concentration ratio is defined as follows [9]

$$n = \frac{p_p}{p_s}. \tag{25}$$

Substituting Eq. (24) in Eq. (25) yields

$$n = \frac{m_p(1-m_{cp})}{m_{cp}(1-m_p)}\left[1 + \frac{1}{\frac{2C_c p}{U_1'(l_1+l_0)} - m_p}\right]. \tag{26}$$

Some observations from Eq. (26) are made:

(a) A small embankment load (p) results in $l_0 + l_1 \to 0$, consequently, n approaches 1.0. This is consistent with field observations because the differential settlement between the pile and soil is limited under a light load owing to the cushion layer.

(b) When the embankment load is extremely heavy ($p \to \infty$), n approaches 1.0. This can be attributed

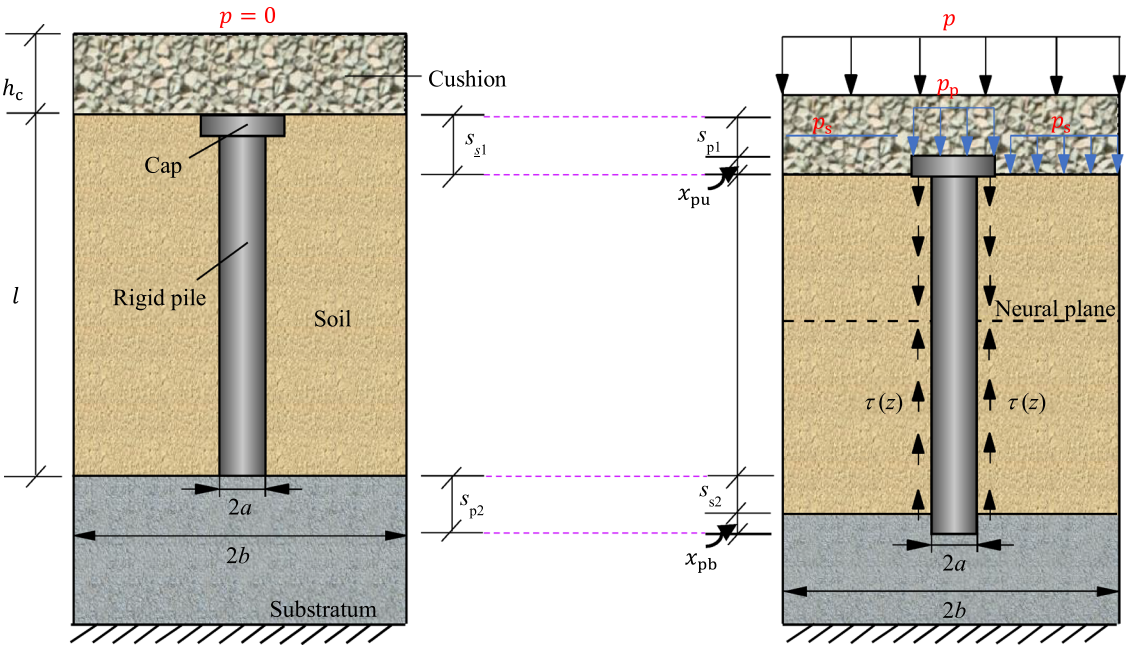

Fig. 6 Schematic of displacement compatibility given the pile penetration under applied loads

to that the foundation settlement becomes extremely large as the pile group reaches a failure state, and the effect of stiffness difference between the pile and soil on the mechanical response of the pile–soil system is less pronounced.

(c) When the cushion layer is completely flexible ($C_c \to \infty$), n approaches 1.0 without pile cap.

4 Case study

Two cases obtained from the literature were used to validate the proposed analytical solution. Case 1 was reported by Zhang et al. [44], and Case 2 was numerically performed by Chen et al. [8]. The parameters required in the analysis of the two cases are summarized in Table 1. The load share ratio was used in abovementioned documents, defined as the proportion of total embankment load carried by the piles. A relationship is established between and stress concentration ratio (n) as follows:

$$R_p = \frac{1}{1 + \frac{1-m_{cp}}{n \cdot m_{cp}}} \times 100\%. \tag{27}$$

An alternative approach was used for identifying parameters K_0, U_1', U_2', C_c, and C_r, which are unavailable from the literature. The value of was estimated based on [45] or can be obtained through a back analysis of direct shear test results [31, 46–49], ranging from 0.1% to 2% for various soil types. C_c and C_r were estimated using the empirical formulae reported by Wu et al. [50] as follows:

$$C_c = \frac{h_c}{E_c}, \tag{28}$$

$$C_r = \frac{(1 - v_r^2)\xi\sqrt{A_r}}{E_r}, \tag{29}$$

where h_c and E_c are the thickness and constrained modulus of the cushion layer, respectively; ξ is an empirical coefficient (0.8 for soft soil and 1.2 for stiff soil); A_r is the cross-sectional area of the pile tip; E_r and v_r represent the constrained modulus and Poisson's ratio for the stratum, respectively.

4.1 Case 1

Zhang et al. [44] reported a field test performed on piled embankments over silty clay of medium compressibility. The embankment has been reinforced by cement-fly ash-gravel (CFG) piles and a geogrid layer over pile caps. Field measurements presented little tension in the geogrid layer, approximately 8–10 kN/m. The geosynthetic reinforcement contributed little to the load redistribution on the pile cap and soil surface beneath the cushion layer. The results of two test sections, G1 and G3, were used in this study for validation. It is noteworthy that all piles were floating and arranged in an equilateral triangular pattern with a circular cap.

Table 1 Parameters of interest in the analysis for Cases 1 and 2

	Material	Physical and mechanical properties	N.G.	
			Values	Method
Case 1	Embankment	h_f =11.5 m (G1), 12.2 m (G3); γ_f =20 kN/m^3	p = 230 kPa (G1), 244 kPa (G3)	$p = \gamma_f \cdot h_f$
	Cushion	h_c =0.5 m; γ_c =20 kN/m^3; E_c=30 MPa	C_c = 1.67×10^{-5} m/kPa	Eq. (28)
	Pile	l=8 m (G1), 12 m (G3); S=1.8 m (G1), 2.0 m (G3); d=0.5 m; d_{cap}=1.0 m; E_p=20 GPa	b=0.945 m (G1), 1.05 m (G3)	Eq. (9)
	Adjacent soil	h_s=8 m (G1), 12 m (G3); γ_s=19.0 kN/m^3; c_s=30 kPa; φ_s=35°; E_s=30 MPa; v_s=0.35	c_a=21 kPa φ_a=24.5° $U_1' = U_2'$ =2.5‰ K_0=0.70	Eq. (4a) Eq. (4b) Interface shear test [45]
	Substratum	H=12 m; γ_{sb} =19.0 kN/m^3; c_{sb} =30 kPa; φ_{sb}=25°; E_{sb}=30 MPa; v_{sb}=0.35	C_r =1.61×10^{-5} m/kPa	Eq. (29)
Case 2	Embankment	h_f =4 m; γ_f =20 kN/m^3	p = 80 kPa	
	Cushion	h_c =0.5 m; γ_c =20 kN/m^3; E_c=30 MPa	C_c = 1.67×10^{-5} m/kPa	Eq. (28)
	Pile	l=20 m; d=0.4 m; S=2.5 m; d_{cap}=1.13 m; E_p=35 GPa	b = 1.41 m	Eq. (9)
	Adjacent soil	h_s=20 m; γ_s=17.5 kN/m^3; c_s=15 kPa; φ_s=9°; E_s=2.2 MPa; v_s=0.35	c_a = 10.5 kPa φ_a = 6.3° $U_1' = U_2'$=1.4‰ K_0=0.65	Eq. (4a) Eq. (4b) Interface shear test [45]
	Substratum	H=5 m; γ_{sb} =17.5 kN/m^3; c_{sb} =15 kPa; φ_{sb}=9°; E_{sb} =2.2 MPa; v_{sb}=0.35	C_r = 1.27×10^{-4} m/kPa	Eq. (29)

N.G. = Not given in reference; h_f = height of embankment; γ_f = unit weight of fill; p = embankment load; h_c = cushion height; γ_c = unit weight of cushion; E_c = constrained modulus of cushion; C_c = flexibility factor of cushion; l = pile full length; d = pile diameter; S = pile spacing; E_p = Young's modulus of pile; d_{cap} = diameter of pile cap; b = radius of analysis element; h_s = thickness of soil between piles; γ_s = unit weight of surrounding soil; c_s = effective cohesion of adjacent soil; φ_s = effective friction angle of adjacent soil; v_s = Poisson's ratio of adjacent soil; c_a = adhesion of pile–soil interface; φ_a = friction angle of pile–soil interface; E_s = constrained modulus of surrounding soil; U_1', U_2' = ultimate relative pile–soil displacement per unit length; K_0 = lateral earth pressure coefficient; γ_{sb} = unit weight of substratum; c_{sb} = effective cohesion of substratum; φ_{sb} = effective friction angle of substratum; E_{sb} = constrained modulus of substratum; v_{sb} = Poisson's ratio of substratum; C_r = flexibility factor of substratum. G_1 to G_3 denote different test sections.

Figure 7 demonstrates the comparisons between the computed and measured values of the load share ratio from Sections G1 and G3. Three specifications were involved, namely Britain's BS8006 design code, Nordic handbook (NGG) [19], and EBGEO [51]. It is clear that the proposed method yielded satisfactory predictions, while the remaining methods generally overestimated the value of R_p. The primary causes were that some fundamental factors for the mechanism of load transfer, such as pile penetration behavior and skin friction distribution, have been included in the analytical solution. In addition, different approaches to account for the function of the cushion layer have

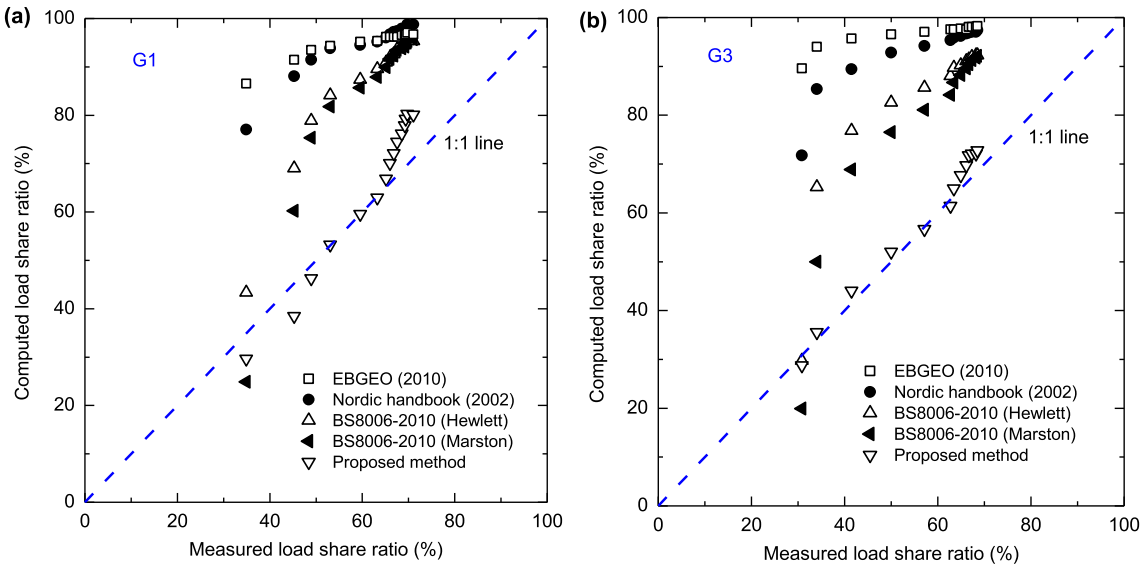

Fig. 7 Measured values vs. computed values for the load share ratio (R_p) in Sections G1 (**a**) and G3 (**b**)

significantly affected the computed results, at least in the case of a high embankment. Generally, the present method demonstrates promise in determining stress concentration ratio in engineering practice.

4.2 Case 2

In the second scenario, a numerical simulation [8] was performed on a rigid pile-supported embankment without geosynthetic reinforcement over soft soil based on the commercial software PLAXIS. An axisymmetric model was established to represent the unit cell introduced in Fig. 4, i.e., a cylindrical soil column incorporating a single pile. Other details regarding the development of the numerical model can be found in [8].

The results of numerical simulation, Chen's method [8], and the analytical solution in this study were compared in terms of the skin friction distribution along the pile shaft (Fig. 8). The skin friction varied similarly for all three methods, and the distribution pattern was consistent with the concept of three segments introduced in Fig. 3. Compared with Chen's method, the present method agreed well with the simulation results when the ultimate state reached the pile–soil interface.

Figure 9 demonstrates the profile of relative displacement between the pile and adjacent soil from the analytical solution. The pile penetrations at the head and tip are 9.52 and 14.28 mm, respectively. Based on Eqs. (22) and (23), the differential settlement at the pile cap can be obtained as 23.8 mm, similar to the results of numerical analysis

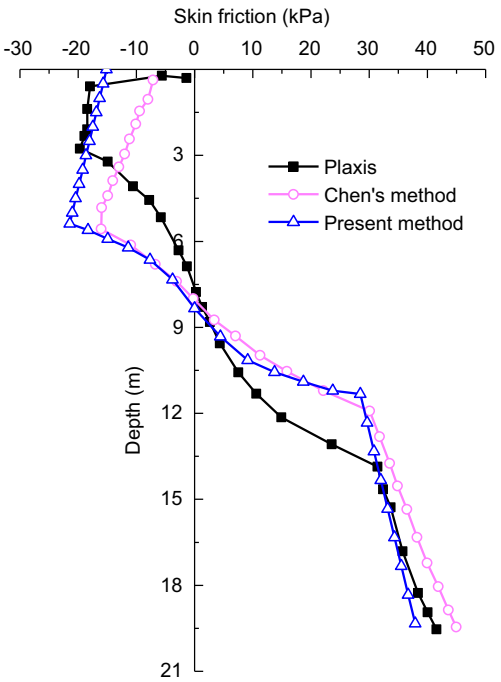

Fig. 8 Comparison of calculated distributions of skin friction along the pile shaft [8]

(20.0 mm) and Chen's method (24.0 mm). The load share ratio (R_p) and elevation level of the neutral plane are presented in Table 2, which allows the present solution to be validated.

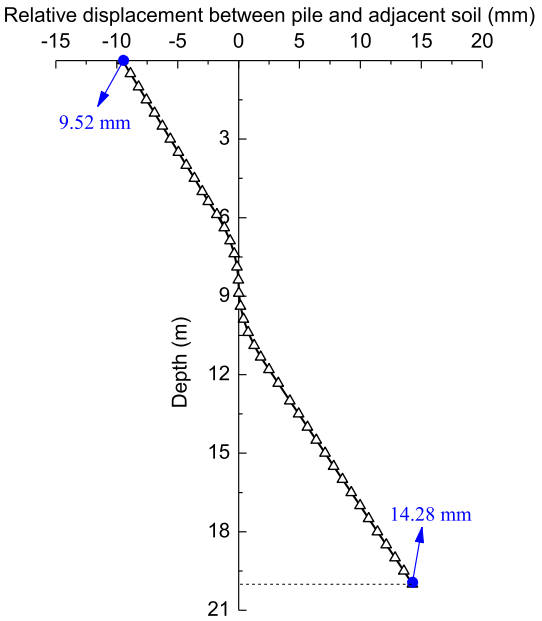

Fig. 9 Relative displacement between surrounding soil and pile varying with depth in Case 2 using the present method

Table 2 Comparison between three methods in Case 2 regarding the results of load share ratio and neutral plane location

Method	Load share ratio R_p (%)	Depth of neutral plane l_0 (m)
FEM	66.7	7.79
Chen's method	74.0	8.05
Present method	64.2	8.35

5 Concluding remarks

A simple analytical framework was presented for estimating the stress concentration ratio of piled embankment considering the mechanical response of pile–soil system. Two application scenarios reported in existing literature were used to validate the proposed method. The following conclusions were obtained:

(1) The fast algorithm provided rational estimations for the load share ratio, skin friction distribution, location of neural plane, and differential settlement between the pile cap and the adjacent soils.

(2) The pile–soil interaction, stiffness of cushion layer, and pile penetration behavior were crucial for the identification of stress concentration ratio of piled embankments.

(3) The current method offers benefits such as easy access of parameters with clear physical meanings, affording well understanding of the impact of cushion stiffness on stress concentration ratio, and the consideration of pile–soil interaction.

Although the present algorithm yielded reliable predictions, it should only be treated as a simplified approach and a general guide to the field response. Future work is to deal with arching and an advanced model for geosynthetic reinforcement, and reduce the assumptions and simplifications to handle more complex situations. Despite such limitations, this study serves as a fast algorithm for the determination of stress concentration ratio on the design aspects.

Acknowledgments This work was supported by the National Natural Science Foundation of China (Grant Nos. 52078435 and 41901073), Shanghai Key Laboratory of Rail Infrastructure Durability and System Safety (Grant No. R202003), and China Postdoctoral Science Foundation (Grant No. 2019M663556).

References

1. Bian X, Li W, Hu J, Liu H, Duan X, Chen Y (2018) Geodynamics of high-speed railway. Transp Geotech 17:69–76
2. Zhou M, Liu H, Chen Y, Hu Y (2016) First application of cast-in-place concrete large-diameter pipe (PCC) pile-reinforced railway foundation: a field study. Can Geotech J 53:708–16
3. Zhou S, Wang B, Shan Y (2020) Review of research on high-speed railway subgrade settlement in soft soil area. Railw Eng Sci 28:129–145
4. Zheng G, Jiang Y, Han J, Liu Y (2011) Performance of Cement-fly Ash-gravel Pile-supported High-speed Railway embankments over soft marine clay. Mar Georesources Geotechnol 29:145–61
5. Wang C, Xu Y, Dong P (2014) Working characteristics of concrete-cored deep cement mixingpiles under embankments. J Zhejiang Univ Sci A 15:419–31
6. Wu L, Jiang G, Ju N (2019) Behavior and numerical evaluation of cement-fly ash-gravel pile-supported embankments over completely decomposed granite soils. Int J Geomech 19:04019048

7. Zhuang Y, Cui X (2016) Case studies of reinforced piled High-speed railway embankment over soft soils. Int J Geomech 16:06015005
8. Chen R, Chen Y, Han J, Xu Z (2008) A theoretical solution for pile-supported embankments on soft soils under one-dimensional compression. Can Geotech J 45:611–623
9. Han J, Gabr MA (2002) Numerical analysis of geosyntheticreinforced and pile-supported earth platforms over soft soil. J Geotech Geoenvironm Eng 128:44–53
10. Nunez MA, Briançon L, Dias D (2013) Analyses of a pilesupported embankment over soft clay: full-scale experiment, analytical and numerical approaches. Eng Geol 153:53–67
11. Ariyarathne P, Liyanapathirana DS (2015) Review of existing design methods for geosynthetic-reinforced pile-supported embankments. Soils Found 55:17–34
12. van Eekelen SJM, Bezuijen A, van Tol AF (2013) An analytical model for arching in piled embankments. Geotext Geomembran 39:78–102
13. van Eekelen SJM, Bezuijen A, van Tol AF (2015) Validation of analytical models for the design of basal reinforced piled embankments. Geotext Geomembran 43:56–81
14. Hewlett WJ, Randolph MF (1988) Analysis of piled embankments. Gr Eng 21:12–8
15. Raithel M, Kirchner A, Kempfert HG (2008) German recommendations for reinforced embankments on pile-similar elements. In: Li G, Chen Y, Tang X (eds) Geosynthetics in Civil and Environmental Engineering. Springer, Berlin
16. McGuire M (2011) Critical height and surface deformation of column-supported embankments. Dissertation,Virginia Polytechnic Institute and State University
17. Russell D, Pierpoint N (1997) An assessment of design methods for piled embankments. Gr Eng 30:39–44
18. Collin JG (2004) Column supported embankment design considerations.In: 52nd Annual Geotechnical Engineering Conference. University of Minnesota, Minneapolis, MN, USA, pp. 51–78
19. Nordic Geotechnical Society (2002) Nordic handbook reinforced soils and fills. Nordic Geotechnical Society, Stockholm, Sweden
20. Zhuang Y, Wang K (2018) Finite element analysis on the dynamic behavior of soil arching effect in piled embankment. Transp Geotech 14:8–21
21. Liu W, Qu S, Zhang H, Nie Z (2017) An integrated method for analyzing load transfer in geosynthetic-reinforced and pile-supported embankment. KSCE J Civ Eng 21:687–702
22. Miao L, Wang F, Lv W (2018) A simplified calculation method for stress concentration ratio of composite foundation with rigid piles. KSCE J Civ Eng 22:3263–70
23. Zhuang Y, Wang K (2017) Analytical solution for reinforced piled embankments on elastoplastic consolidated soil. Int J Geomech 17:06017010
24. Luo Q, Lu Q (2018) Settlement calculation of rigid pile composite foundation considering pile-soil relative slip under embankment load. China J Highw Transp 31:20–30. **(in Chinese)**
25. Abusharar SW, Zheng J, Chen B, Yin J (2009) A simplified method for analysis of a piled embankment reinforced with geosynthetics. Geotext Geomembran 27:39–52
26. Pham TA (2020) Analysis of geosynthetic-reinforced pile-supported embankment with soil-structure interaction models. Comput Geotech 121:103438
27. Matyas E, Santamarina JC (1994) Negative skin friction and the neutral plane. Can Geotech J 31:591–7
28. Zhou W, Chen R, Zhao L, Xu Z, Chen Y (2012) A semi-analytical method for the analysis of pile-supported embankments. J Zhejiang Univ Sci A 13:888–94
29. Randolph MF, Wroth CP (1979) Analysis of vertical deformation of Pile groups. Géotechnique 29:423–39
30. Cao W, Wang J, Luo Z, Zhai Y (2012) Settlement calculation method for composite ground considering pile-soil slip under flexible foundation. China J Highw Transp 25:9–16
31. Evgine E, Fakharian K (1996) Effect of stress paths on the behaviour of sand-steel interfaces. Can Geotech J 33:853–65
32. Zhang S, Zhao M, He L (2011) Calculation of settlement of composite foundation with rigid piles under flexible ground. J Highw Transp Res Dev English Ed 5:15–21
33. Lee J, Park D, Choi K (2014) Analysis of load sharing behavior for piled rafts using normalized load response model. Comput Geotech 57:65–74
34. Mandy K, Robert JM, Frits AF (2016) Pile-soil interaction and settlement effects induced by deep excavations. J Geotech Geoenvironm Eng 142:04016034
35. Yin Z, Zhu H, Xu G (1995) A study of deformation in the interface between soil and concrete. Comput Geotech 17:75–92
36. Potyondy JG (1961) Skin friction between various soils and construction materials. Géotechnique 11:339–53
37. Pham HTV, Suleiman MT, White DJ (2004) Numerical analysis of geosynthetic-rammed aggregate pier supported embankments. GeoTrans 2004, ASCE, Los Angeles, p. 657–664
38. Chen R, Wang Y, Ye X, Bian X, Dong X (2016) Tensile force of geogrids embedded in pile-supported reinforced embankment: a full-scale experimental study. Geotext Geomembran 44:157–69
39. SJM Eekelen van (2019) The Dutch design guideline basal reinforced piled embankments, and the development and validation of its design methods Fifteenth International Conference on Structural and Geotechnical Engineering, Cairo, Egypt, 2019. p. 1–17
40. Balaam NP, Poulos HG, Brown PT (1977) Settlementanalysis of soft clays reinforced with granular piles. In: 5th Southeast Asian Conference on Soil Engineering, Bangkok, Thailand, 1977, p. 81–92
41. Ambily AP, Gandhi SR (2007) Behavior of stone columns based on experimental and FEM analysis. J Geotech Geoenvironm Eng 133:405–15
42. Balaam NP, Booker JP (1981) Analysis of rigid rafts supported by granular piles. Int J Numer Anal Methods Geomech 5:379–403
43. Zhao M, He L, Zhang L (2010) Settlement calculation of CFG pile composite foundation based on load transfer method. Rock Soil Mech 31:839–44
44. Zhang C, Jiang G, Liu X, Buzzi O (2016) Arching in geogrid-reinforced pile-supported embankments over silty clay of medium compressibility: field data and analytical solution. Comput Geotech 77:11–25
45. Mayne PW, Kulhawy FH (1982) K0-OCR relationship in soil. J Geotech Engrg Div 108:851–72
46. Hu L, Pu J (2004) Test and modeling of soil-structure interface. J Geotech Geoenvironm Eng 130:851–60
47. Shakir RR, Zhu J (2009) Behavior of compacted clay-concrete interface. Front Struct Civ Eng 3:85–92
48. Jason T, Zachary J (2009) Role of initial state, material properties, and confinement condition on local and global soil-structure interface behavior. J Geotech Geoenvironm Eng 133:1646–60
49. Pra-Ai S, Boulon M (2017) Soil-structure cyclic direct shear tests: a new interpretation of the direct shear experiment and its application to a series of cyclic tests. Acta Geotech 12:107–27
50. Wu C, Guo W, Li Y, Tie R (2016) Calculation of neutral surface depth and pile-soil stress ratio of rigid pile composite foundation considering influence of negative friction. Chinese J Geotech Eng 38:278–87. **(in Chinese)**
51. German Geotechnical Society (2010) Empfehlungen für den entwurf und die berechnung von erdkörpern mit bewehrungen aus geokunststoffen– EBGEO (Recommendation for design and analysis of earth structures using geosynthetic reinforcements). Ernst Sohn Berline. **(in German)**